Development of Surface Fluorescence X-ray Absorption Fine Structure using a Laue-type Monochromator and its Application to Sub-Monolayer-Coverage Surface in Solution

Yuki Wakisaka[a], Daiki Kido[a], Hiromitsu Uehara[a], Qiuyi Yuan[a], Felix E. Feiten[a], Shingo Mukai[a], Satoru Takakusagi[a], Yohei Uemura[b], Toshihiko Yokoyama[b], Takahiro Wada[c], Motohiro Uo[c], Oki Sekizawa[d, e], Tomoya Uruga[d, e], Yasuhiro Iwasawa[d], and Kiyotaka Asakura*[a]

[a] Y. Wakisaka, D. Kido, H. Uehara, Q. Yuan, F. E. Feiten, S. Mukai, S. Takakusagi, K. Asakura
Institute for Catalysis, Hokkaido University
Kita-ku, Sapporo, Hokkaido, 001-0021 (Japan)
E-mail: askr@cat.hokudai.ac.jp
[b] Y. Uemura, T. Yokoyama
Institute for Molecular Science
Myodaiji-cho, Okazaki, Aichi, 444-8585 (Japan)
[c] T. Wada, M. Uo
Graduate School of Medical and Dental Sciences, Tokyo Medical and Dental University,
Yushima, Bunkyo-ku, Tokyo, 113-8549 (Japan)
[d] O. Sekizawa, T. Uruga, Y. Iwasawa
Department of Applied Physics and Chemistry, The University of Electro-Communications
Chofugaoka, Chofu, Tokyo, 182-8585 (Japan)
[e] O. Sekizawa, T. Uruga
Japan Synchrotron Radiation Research (JASRI)
Sayo-cho, Sayo-gun, Hyogo, 679-5148 (Japan)

Supporting information for this article is given via a link at the end of the document.

Abstract: Surface fluorescence X-ray absorption fine structure (FXAFS) using a Laue type monochromator is developed to acquire the structural information of metals with very low concentrations on a flat, highly oriented pyrolytic graphite (HOPG) surface in the presence of electrolytes. Generally, surface fluorescence XAFS is hindered by strong scatterings from the bulk, which often choke the pulse counting detectors. In this work, we show that a bent crystal Laue analyzer (BCLA) can efficiently remove the scattering X-rays coming from the bulk even in the presence of a thick solution layer. We applied the technique to a sub-monolayer (~10^{14} atoms per cm^2) of Pt on HOPG, and have successfully obtained high S/N *in situ* XAFS data in combination with BI (back-illuminated)-FXAFS. This technique allows us to carry out *in situ* XAFS measurements of a flat electrode surface in the presence of electrolytes.

1. Introduction

Nanoparticles (NPs) deposited on solid substrates (oxide and carbon) play an important role in catalysts, sensors, fuel cells, and electrodes. The structures of the deposited metal NPs are often investigated by X-ray absorption fine structure (XAFS) because they are highly dispersed on the substrate surface and diffraction techniques are less effective.[1] If the substrates are in powder form, such as SiO_2 and Al_2O_3 used as catalyst supports, the surface area is typically large, and conventional transmission XAFS can be applied.[1-2] If flat substrates are used, such as single crystal surfaces, and the NPs are located only on their surfaces, the three-dimensional interface structure and interaction between the NPs and substrates can be obtained using polarization dependent XAFS analysis.[3] However, the surface concentration of metal atoms on flat surfaces can be as small as $10^{14–15}$ cm^{-2} and the scattering X-ray intensity from the bulk is too large, both of which make it impossible to measure the XAFS with good S/N. To resolve this issue, we have developed a polarization-dependent total reflection fluorescence X-ray absorption fine structure (PTRF-XAFS), which facilitates the determination of three-dimensional structures of highly dispersed sub-monolayer metal atoms (down to 10^{13} cm^{-2}) on flat surfaces.[4] An important nanoparticle system in which the detailed structure is of interest, is the carbon surface covered by Pt NPs used in polymer electrolyte fuel cells (PEFCs).[5] This system is an important fuel-cell catalyst, particularly for cathode reactions such as oxygen reduction.[6] However, the slow kinetics, high overpotential of the cathode reaction, and the degradation of Pt NPs through potential cycles hinder the widespread applications of PEFCs. To increase the activity and stability of the Pt NPs, it is necessary to understand their interface structure and interaction with the carbon electrode. Highly oriented pyrolytic graphite (HOPG) has an atomically flat graphite surface. Therefore, a HOPG surface covered by Pt NPs is a suitable model for a fuel-cell catalyst. However, HOPG has the following critical problems if one uses it as a flat substrate for PTRF-XAFS.

1. On the macro scale, the HOPG surface is not flat enough and it has ripples, which create a considerable amount of elastic scattering.[7]

2. Carbon is a low Z element and requires a smaller glancing angle than that for SiO_2, TiO_2, and Al_2O_3.

It is therefore very difficult to apply PTRF-XAFS to the study of Pt NPs on HOPG substrates.[7]

The total reflection condition is necessary because we have to reduce the strong background scattering coming from the substrate bulk, which hinders the very weak measured fluorescence signal with a high S/B ratio.[3] If the background scattering X-rays are removed efficiently, the total reflection condition is not essential. Solid state detectors (SSDs) have sufficient energy resolution to separate the fluorescent X-rays from the scattering X-rays. However, the maximum count rate may be ~200,000 cps per channel so that the detector will be choked when the stronger X-ray scattering from the bulk is accepted.

The other way to separate fluorescence from the scattering X-rays is to use crystal monochromators.[8] Johann or Johansson type energy analyzers are often used with an energy resolution as high as about 1 eV. Friebel et al. have reported high energy resolution fluorescence detection XAFS (HERFD-XAFS) on the Pt NPs on Rh(111).[9] To distinguish the fluorescent X-rays from the scattering X-rays, a very high energy resolution is not required. Instead, a large solid angle for detection is desirable for highly sensitive measurements. This is very important for fuel-cell investigations because extremely intense X-rays damage the fragile organic polymers (Nafion) used in the cell. A bent crystal Laue analyzer (BCLA) is a crystal monochromator with a large solid angle and moderate energy resolution. In the BCLA, a Si single crystal is curved in a logarithmic spiral.[10] We applied a BCLA to check the possibility of measuring XAFS of 1 monolayer (ML) Pt NPs dispersed on carbon (HOPG) in a back-illuminated (BI) configuration.[7] In the BI configuration, thin HOPG is used as an X-ray window, which has a small absorption of X-rays. In this configuration, the absorption by the solution can be neglected. However, the signal obtained with the BCLA is not sufficient to obtain the extended XAFS (EXAFS) spectra with an acceptable S/N ratio, despite using intense X-rays coming from a tapered undulator in the Photon Factory Advanced Ring (PF-AR, KEK, Tsukuba, Japan).[7]

The reason for this is that the fluorescent X-rays were diffracted only in a small part of the BCLA crystal which is demonstrated by the diffracted X-ray image.[7] The following three causes can be considered.

1. The point source is not sufficiently small. The principle of a BCLA is that all X-rays coming from one point have the same angle to the surface normal of the analyzer at any point of the curve. Once the angle satisfies the Bragg condition, all other X-rays also simultaneously satisfy the Bragg condition. The X-rays coming from the PF-AR (with an emittance of 300 nmrad) have a 200 μm (V) × 600 μm (H) beam size at the sample position.

2. The source and BCLA positions are not sufficiently adjusted.

3. The logarithmic spiral shape is not precise enough.

A new and cutting-edge beamline, BL36XU, in the Super Photon ring-8GeV (SPring-8, JASRI, Sayo, Japan) has just been constructed and is dedicated to the study of fuel-cell systems.[11] It has a tapered undulator and 4 focusing mirrors to provide X-rays with high intensities and small beam sizes (much less than 100 μm in the energy dispersion or vertical directions). Therefore, it is expected that a stronger diffracted X-ray intensity will be obtained with a BCLA in the BL36XU compared with that of the PF-AR. In this paper, we report the energy-analyzed fluorescence (XAFS) at BL36XU using a BCLA for the surface application, specifically for low-concentration Pt NPs on HOPG in the presence of an electrolyte solution. We also present preliminary results of our home-made BCLA intended to control the spiral shape more precisely.[12]

2. Experiment

The XAFS measurements were performed at BL36XU using a BCLA as a florescence energy monochromator and a 25-element Ge-SSD (Canberra, USA). A pixel-array detector (PILATUS 300K-W; Dectoris, Switzerland) was also used for imaging after the BCLA. The incident X-rays were focused to 38 μm (V) × 377 μm (H) with a photon flux of approximately 2×10^{13} photons per second. The vertical beam size was important to adjust the diffraction conditions at the fluorescent X-ray energies in the BCLA. A commercially available BCLA (0095; FMB Oxford, UK) was adopted for separating the Pt L_α fluorescence (9442 eV) from the scattering X-rays. Its diffraction plane was Si (111) with a crystal asymmetry angle of 19.5°. Mo Soller slits rejected the direct X-rays other than the fluorescent X-rays. We also tested a home-made BCLA as shown in Fig. S1, in which extra beams regulated the Si single crystal to produce a more precise logarithmic shape.

Figure 1 shows the schematics of the *in situ* electrochemical cell and experimental arrangement for the back-illuminated fluorescence XAFS (BI-FXAFS) with the BCLA, as well as a photograph of the cell during the measurement. The electrochemical cell body was made of polychlorotrifluoroethylene (PCTFE, Ø66 mm) to withstand strong acid solutions. A Pt coil and Ag/AgCl (saturated NaCl) were used as the counter and reference electrodes, respectively. The electrodes were inserted into the cell through a glass tube. A circular hole (Ø12 mm) was located at the center of one side of the cell, where the HOPG (SPI Supplies Co., ZYB grade, 20 × 20 mm^2 size) was fixed via a perfluoro O-ring [Fig. 1(b)], and used for the X-ray entrance window. In addition, the HOPG was used as the working electrode and as the support for the Pt. The HOPG thus played three roles at once. The calculated X-ray attenuation length of HOPG at 11600 eV is ca. 3.2 mm. To minimize the attenuation by the window of the incident and fluorescent X-rays, the HOPG substrate was stripped by a scotch tape several times until the thickness became ca. 0.5 mm. A glass window was fixed at the other side to see the inside of the cell.

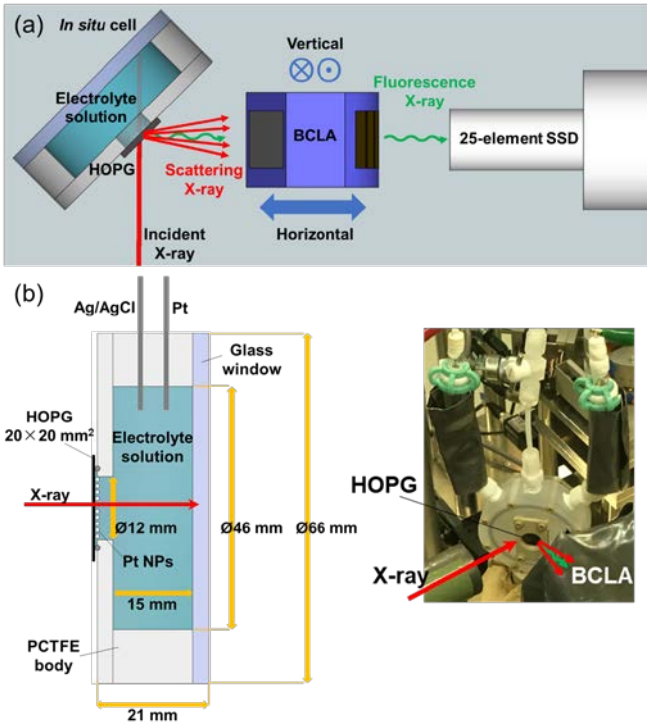

Fig. 1 Schematics of BI-FXAFS. (a) Experimental arrangement and (b) drawing of the *in situ* electrochemical cell (left) and its photograph during the experiment (right). The incident X-rays came from the left side and the fluorescent X-rays were analyzed by the BCLA. The BCLA is covered strictly with lead except its entrance and exit windows.

Dodecanethiol-protected Pt NPs were synthesized and spin-coated onto the HOPG surface in the same way as reported previously.[7] The sample characterization was performed by using transmission electron microscopy (TEM, JEOL, JEM-2100F, Japan) and atomic force microscopy (AFM, Cypher, Asylum, USA). According to the TEM images, the estimated average Pt core diameter was ~1.7 nm, corresponding to Pt_n clusters with ~100 ± 50 atoms, by assuming cuboctaheron shaped NPs. Figure 2 shows a typical AFM picture, where the bright spots are dodecanethiol-protected Pt NPs. The lateral size is overestimated due to the finite tip size effect. Judging from the particle density and size, and assuming that the Pt clusters are stabilized by monolayers of dodecanethiol,[13] the estimated Pt loading was ~5 × 10^{14} cm^{-2} (0.3 ML). The Pt-deposited HOPG was placed in the *in situ* electrochemical cell [Fig. 1(b)] and subjected to cyclic voltammetry (CV) measurements in a 0.1 M $HClO_4$ electrolyte solution. The dodecanethiol layers were removed *in situ* by 50 oxidation-reduction cycles (with a sweeping range from -0.2 to 1.2 V at a rate of 0.05 V/s) before the measurements.[7]

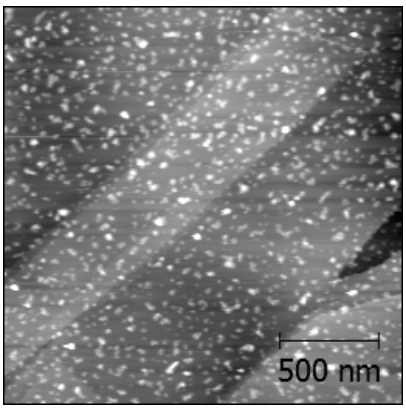

Fig. 2 AFM image of the dodecanethiol-protected Pt NPs on HOPG.

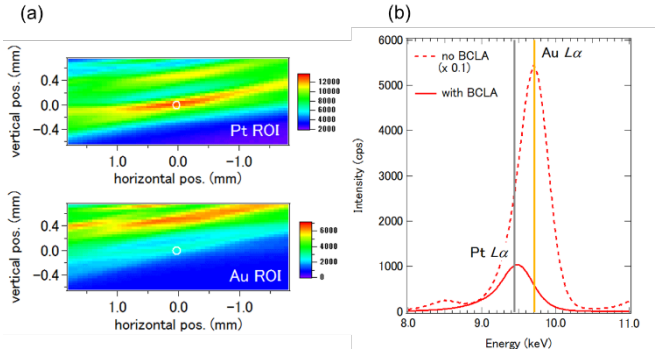

Fig. 3 Optimization of the BCLA position using an AuPt reference sample (Pt/Au = 1/10). (a) Two-dimensional color plots of the Pt L_3 (top) and Au L_3 (bottom) fluorescence intensity summed over all SSD elements. (b) The emission X-ray spectra with and without the use of BCLA. The grey and yellow lines indicate the positions of the Pt and Au L_α lines, respectively.

3. RESULTS and DISCUSSION

3.1. Performance and adjustment of BCLA

The BCLA performance strongly depends on the spot size at the sample and positioning of the BCLA relative to the emission source. The beam size of the BL36XU was 1/10 that of the NW2A at PF-AR in the vertical direction. In order to set the BCLA to the right position and to evaluate its performance, an AuPt reference sample was prepared; a BN pellet mixed with Au and Pt chlorides with an atomic ratio of Pt/Au = 1/10. A failure to align the BCLA correctly leads to detection of the Au peak by most of the SSD elements with an incident X-ray energy above the Au L_3 edge. Figure 3 is an example of the evaluation of the BCLA position optimization. Figure 3(a) shows two-dimensional color plots of the Pt L_α (top) and Au L_α (bottom) fluorescence intensity summed over all SSD elements using the AuPt reference sample. The incident X-ray energy was set at 12.1 keV, above the Au L_3 edge. When the BCLA height was increased, the Pt L_α first appeared, followed by a strong Au L_α intensity. The optimum BCLA position was set to the point represented by the white circle in Fig. 3(a), at which we could obtain the maximum intensity for the Pt L_α fluorescence and a relatively weak intensity for the Au L_α fluorescence after the Au L_3 edge. Figure 3(b) shows the pulse height analysis of the output coming from one element in the multi SSD with and without BCLA. Without BCLA, only the Au L_α fluorescence was observed, obscuring the Pt L_α fluorescence. After inserting the BCLA, the Pt L_α fluorescence was observed, indicating that the BCLA effectively removed the strong Au fluorescence.

Figure 4 shows images of the X-ray intensity behind the BCLA using PILATUS. In Fig. 4(a) (viewed from PILATUS), Pt L_α fluorescent X-rays were observed at a larger area than in the BCLA experiment at NW2A in PF-AR, as shown in Fig. 4(b). However, not the entire area was bright, indicating some parts were not diffracted properly. The right side of Fig. 4(a), indicated by the red arrow, was dark due to the finite width of the BCLA. In addition, the region marked by the red circles at the left side in Fig. 4(a) showed only small intensities of Pt fluorescence. When the X-ray energy was tuned above the Au L_3 edge (12.1 keV), the Au peak was detected (Fig. S3).

Figure 5(a) shows the pulse height analyses of the outputs coming from each SSD element when the sample was excited at 12.1 keV. Five out of the 25 elements of the multi SSD did not accept fluorescent X-rays due to the small width of the BCLA. This corresponds well to the dark area at the right side of Fig. 4(a). Sixteen elements accepted X-rays with energies corresponding to Pt L_α fluorescence and four other elements detected X-rays with energies corresponding to Au L_α fluorescence or both Pt and Au L_α fluorescence, as shown in Fig. 5(a). The positions of these 4 elements [1, 2, 5, and 10 shown in Fig. 5(b)] correspond to dark domains of BCLA images as shown in the red circles in Fig. 4(a). For further spatial correspondence between the multi SSD and PILATUS see Figs. S3 and S4 in the Supporting Information.

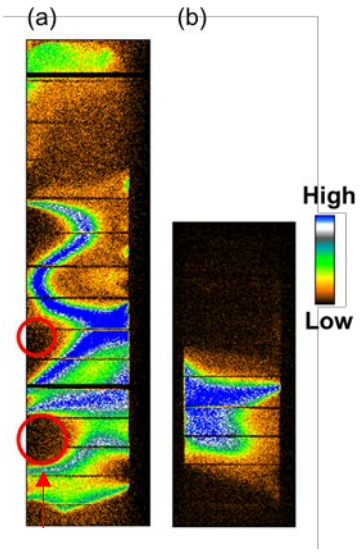

Fig. 4 PILATUS images behind the BCLA. Pt L_α florescent X-rays were emitted from reference samples. The incident X-ray energy was 11.6 keV, which is above the Pt L_3 edge. (a) Imaged using PILATUS 300K-W at BL36XU. (b) Imaged previously using PILATUS 100K at NW2A in PF-AR[7] (thus the image size is small). The red circles represent the areas where the Pt L_α florescence X-rays were not detected.

Figure S2 shows the pulse height analyses of the output from the SSD elements for the same sample using the home-made BCLA. All 25 elements detected Pt L_α fluorescent X-rays, implying that the home-made BCLA has a larger acceptance angle to cover the multi SSD detectors. In addition, the logarithmic spiral shape might be more precisely bent[12] due to the arrangement of the beams in a logarithmic spiral way as shown in Fig. S1.

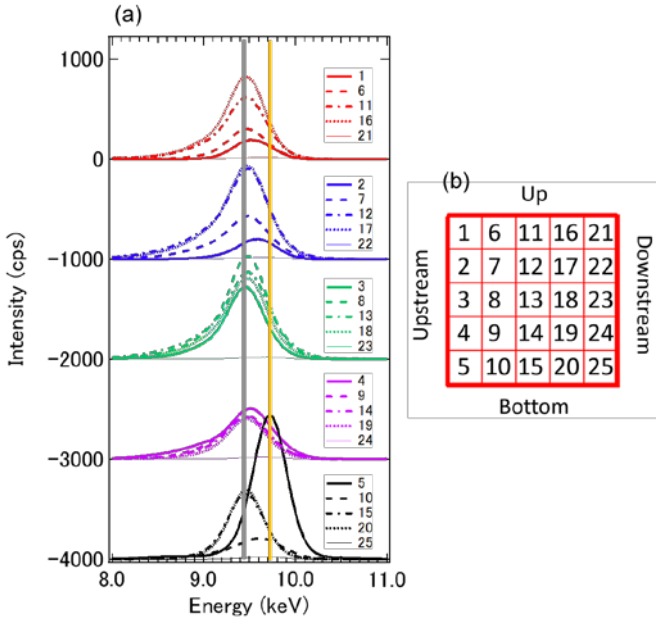

Fig. 5 (a) Pulse height analysis of outputs coming from each element of the multi SSD after the commercial BCLA. The sample was AuPt (Pt/Au=1/10) and the incident X-ray energy was 12.1 keV. The grey and yellow lines indicate the positions of the Pt and Au L_α lines, respectively. (b) The spatial positions of all SSD elements arranged in a 4 cm × 4 cm square (viewed from the SSD, see also Fig. S4).

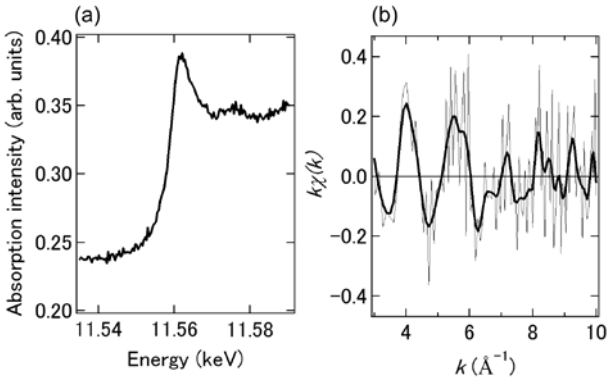

Fig. 6 *In situ* Pt L_3-edge XAFS spectra of the Pt NPs on the HOPG at 0.53 V vs Ag/AgCl in 0.1 M $HClO_4$ solution. (a) Raw XANES and (b) EXAFS (thin line) overlaid by its smoothed spectrum (thick line).

3.2. Application to Pt NPs on the HOPG

The sample was changed to the HOPG with a 10^{14}-cm^{-2}-order Pt loading after optimization of the BCLA position. Figures 6(a) and 6(b) show the X-ray absorption near the edge structure (XANES) and EXAFS spectra, respectively, for the Pt NPs contacting the electrolyte. The incident X-ray angle was 45°. The sample potential was fixed at the rest potential; 0.53 V vs Ag/AgCl in 0.1 M $HClO_4$. Compared to the previously reported data which were measured at the PF, the S/N ratio was much improved.[7] The total accumulation time for the EXAFS spectrum was approximately 2 hours. We previously spent 4 hours to measure only the XANES region. To the best of our knowledge, this is the first time the EXAFS of sub-monolayer metal atoms (10^{14}-cm^{-2}-order), dispersed on a low Z substrate in contact with a thick solution layer without using total reflection, have been obtained. An accumulation time of 2 hours is a reasonable time scale, comparable to the total reflection fluorescence method. We conclude that we can thus measure the EXAFS of low coverage Pt on a HOPG surface in the presence of electrolyte using a BCLA and BI-XAFS. Note that the background level is high, implying that the inelastic X-ray level is high. Strong inelastic X-ray scattering limits the lowest detection level.

4. Summary

We have improved the fluorescence XAFS method and successfully measured the sub-monolayer-coverage Pt NPs dispersed on a HOPG using a BCLA combined with highly brilliant X-rays and precise two-dimensional BCLA position adjustment. The previous low throughput of the BCLA used at PF/PF-AR[7] was due to the focus size and insufficient alignment of the BCLA. The logarithmic spiral Laue analyzer requires a vertically small source size since it is necessary to guarantee that the incident angle into the BCLA crystal is constant. We previously used PF-AR with an emittance of ~300 nmrad, and the focus was poor [200 μm (V) × 600 μm (H)]. In SPring-8, the focus size is ~38 μm (V) × 377 μm (H). Moreover, taking advantage of this small focus size, the BCLA position was precisely adjusted with two-dimensional scans. This alone would not be enough to obtain X-ray diffraction from the whole area of the BCLA, as seen in Figs. 4 and 5(a). When the crystal was more precisely bent, according to the logarithmic spiral curve, the detection throughput and diffraction area could be improved. Our preliminary results using the home-made BCLA actually show better diffraction conditions, allowing fluorescent X-rays corresponding to the Pt L_α peak to enter all SSD elements as shown in Fig. S2.[12]

5. Future Aspects for Fuel Cell Applications

The BCLA is a filter to select the energy around the fluorescence X-ray. Thus the fluorescence can in principle be detected with a high S(signal)/B(background) ratio. Figure 6 shows the raw data with an S/B ratio of only 1.5. The origin of the background is inelastic scattering X-rays mainly from the water. The fluorescence peak did not clearly appear in the emission energy spectra in the SSD signal. This implies that a large inelastic background was present in this region. Because the energies of the inelastic scattering and fluorescence signal were similar, it would be difficult to increase the S/B ratio in the BCLA.

We have to use an electrolyte layer with a thickness of the order of a few mm in a BI (back illuminated) configuration. Judging from the attenuation length (a few mm) the appropriate thickness might be 1 mm which allows sufficient material diffusion and small X-ray scattering.

Even with this limitation, the use of BCLA offers a new approach to surface EXAFS of metal atoms on flat substrates under ambient pressure. Traditionally, there are two main detection methods: Auger electron yield and PTRF-XAFS. The former method is essentially surface sensitive because the escape depth of Auger electrons is only a few nm. However, the Auger electron yield XAFS has a low S/B ratio due to the scattered electrons and secondary electron background, and the photoelectron peak interferes with the XAFS signal.[14] Its application is even more difficult for *in situ* measurements. Although *in situ* photoelectron measurements of fuel-cell catalysts have been reported,[15] *in situ* XAFS using Auger detection from Pt NPs on an HOPG in contact with a solution is still very challenging. In PTRF-XAFS, the total reflection is used and the X-rays can propagate a few nm from the surface as described in the introduction. As the solution has a high transparency to hard X-rays, it can easily be applied to surface measurements in the presence of a solution.[16] However, since it requires a high degree of surface flatness with a large area (cm size along the beam direction), the flatness of the HOPG surface on a macro scale is not sufficient to apply the PTRF-XAFS to the HOPG surface.

Here, we have demonstrated the possibility of observing fluorescence XAFS using a BCLA for a sub-monolayer-coverage surface in solution. The fluorescence XAFS using a Laue-type monochromator method has several merits; one of these is that it does not need total reflection conditions. A polarization-dependent XAFS is also possible if the orientation of the substrate can be changed. In our system, the HOPG can be used as a window and the XAFS of the Pt measured in a BI way, which is termed BI-FXAFS.[7] The combination of the BCLA and BI-FXAFS for Pt on HOPG is the third method to carry out the surface structure analysis in solution under reaction conditions.

A further merit of the BCLA and BI-XAFS is observed when it is applied to a PtAu nanoparticle dispersed on HOPG. The PtAu nanoparticle showed high specific oxygen reduction reaction (ORR) activity.[17] Usually, it is difficult to measure the Pt L3-edge EXAFS of PtAu alloy NPs because the Au L3 absorption edge deteriorates the Pt L3 edge EXAFS. The difference of the two edges is 350 eV (the Au edge appears around 9.2 $Å^{-1}$ [18]) so that the K-edge EXAFS measurement is necessary to obtain the full range of EXAFS.[19] Although the BCLA can separate the Au L3 fluorescence from that of the Pt fluorescence, the part of the X-ray to excite Pt will be absorbed by Au and the dip appears in the spectrum if the Au concentration is high. However, the PtAu nanoparticle on HOPG has a very low concentration so that no absorption of Au affects the Pt EXAFS and we can measure the Pt L3 edge without any interference of Au.[20]

Further enhancement in sensitivity would be achieved in mildly grazing incidence geometry; the incident angle is a few degrees larger than the critical angle.[16d, 21]

The combination of BCLA and BI XAFS is a powerful technique in investigating the Pt nanoparticle deposited on HOPG model system.

Acknowledgements

The authors would like to express their gratitude to the New Energy and Industrial Technology Development Organization (NEDO) PEFC project for their financial support. In addition, two of the authors were supported by the Cooperative Research Program of Institute for Catalysis, Hokkaido University (Nos. 14B1008 and 15A1004 for Y.U.; and Nos. 14B1007, 15A1003 16B1004, and 17B1007 for T.W.). Felix E. Feiten was supported by the Japanese Society for the Promotion of Science and the Alexander von Humboldt Stiftung. We are also supported by the Grant-in-Aid for Scientific Research from JSPS (16F1679507). We thank Mr. Y. Niwa, Dr. H. Nitani, and Dr. H. Abe at the PF of the Institute for Materials Structure Science, and Prof. G. Bunker for fruitful discussions regarding the BCLA. The XAFS measurements were performed under project number 2016A7902 at SPring-8, and preliminary studies were performed at the PF under the approval of PAC No. 2014G040.

Entry for the Table of Contents (Please choose one layout)

Layout 1:

PERSONAL ACCOUNT

Text for Table of Contents

((Insert TOC Graphic here))

*Author(s), Corresponding Author(s)**

Page No. – Page No.

Title

[1] Y. Iwasawa, K. Asakura, M. Tada, Springer, **2016**.
[2] F. W. Lytle, G. H. Via, J. H. Sinfelt, *J. Chem. Phys.* **1977**, *67*, 3831.
[3] K. Asakura, in *Catalysis Vol. 24* (Eds.: J. J. Spivey, M. Gupta), RSC publishing, Cambridge, **2012**, pp. 281–322.
[4] aM. Shirai, T. Inoue, H. Onishi, K. Asakura, Y. Iwasawa, *J. Catal.* **1994**, *145*, 159–165; bK. Asakura, W. J. Chun, M. Shirai, K. Tomishige, Y. Iwasawa, *J.Phys.Chem.* **1997**, *101*, 5549-5556; cW. J. Chun, K. Asakura, Y. Iwasawa, *Chem. Phys. Lett.* **1998**, *288*, 868–872; dK. Ijima, Y. Koike, W. J. Chun, Y. Saito, Y. Tanizawa, T. Shido, Y. Iwasawa, M. Nomura, K. Asakura, *Chem. Phys. Lett.* **2004**, *384*, 134–138; eY. Koike, K. Ijima, W. J. Chun, H. Ashima, T. Yamamoto, K. Fujikawa, S. Suzuki, Y. Iwasawa, M. Nomura, K. Asakura, *Chem. Phys. Lett.* **2006**, *421*, 27–30; fY. Koike, K. Fujikawa, S. Suzuki, W. J. Chun, K. Ijima, M. Nomura, Y. Iwasawa, K. Asakura, *J. Phys. Chem. C.* **2008**, *112*, 4667–4675; gW. J. Chun, K. Miyazaki, N. Watanabe, Y. Koike, S. Takakusagi, K. Fujikawa, M. Nomura, K. Asakura, *J. Ceram. Soc. Jpn.* **2011**, *119*, 890–893; hW.-J. Chun, K. Miyazaki, N. Watanabe, Y. Koike, S. Takakusagi, K. Fujikawa, M. Nomura, Y. Iwasawa, K. Asakura, *J. Phys. Chem. C.* **2013**, *117*, 252–257; iJ. D. Kistler, P. Serna, K. Asakura, B. C. Gates, in *X-Ray Absorption and X-Ray Emission Spectroscopy* (Eds.: J. A. Van Bokhoven, C. Lamberti), John Wiley & Sons, Ltd, **2016**, pp. 773–808; jS. Takakusagi, W.-J. Chun, H. Uehara, K. Asakura, Y. Iwasawa, *Top Catal* **2013**, *56*, 1–11; kS. Takakusagi, A. Kunimoto, N. Sirisit, H. Uehara, T. Ohba, Y. Uemuara, T. Wada, H. Ariga, W.-J. Chun, Y. Iwasawa, K. Asakura, *J. Phys. Chem. C.* **2016**, *120*, 15785–15791.
[5] S. Srinivasan, *Fuel cells: from fundamentals to applications*, Springer Science & Business media, **2006**.
[6] A. Wieckowski, J. K. Norskov, *Fuel Cell Science: Theory, Fundamentals, and Bioatalysis, Vol. 9*, John Wiley and Sons, **2011**.
[7] H. Uehara, Y. Uemura, T. Ogawa, K. Kono, R. Ueno, Y. Niwa, H. Nitani, H. Abe, S. Takakusagi, M. Nomura, Y. Iwasawa, K. Asakura, *Phys. Chem. Chem. Phys.* **2014**, *16*, 13748; H. Uehara, Y. Uemura, T. Ogawa, K. Kono, R. Ueno, Y. Niwa, H. Nitani, H. Abe, S. Takakusagi, M. Nomura, Y. Iwasawa, K. Asakura, *Phys. Chem.* 13754.
[8] aT. Mochizuki, K. Kakinuma, M. Uchida, S. Deki, M. Watanabe, K. Miyatake, *Chem. Sus. Chem.* **2014**, *7*, 729–733; bG. Bunker, *Introduction to XAFS: a practical guide to X-ray absorption fine structure spectroscopy*, Cambridge University Press, **2010**.
[9] D. Friebel, V. Viswanathan, D. J. Miller, T. Anniyev, H. Ogasawara, A. H. Larsen, C. P. O'Grady, J. K. Nørskov, A. Nilsson, *J. Am. Chem. Soc.* **2012**, *134*, 9664–9671.
[10] aA. Kropf, R. J. Finch, J. A. Fortner, S. Aase, C. Karanfil, C. U. Segre, J. Terry, G. Bunker, L. D. Chapman, *Rev. Sci. Instrum.* **2003**, *74*, 4696; bY. Sakayanagi, *Japanese Journal of Applied Physics* **1982**, *21*, L225–L226; cZ. Zhong, L. D. Chapman, B. A. Bunker, G. B. Bunker, R. Fischetti, C. U. Segre, *J.Synchro. Rad.* **1999**, *6*, 212–214.
[11] O. Sekizawa, T. Uruga, M. Tada, K. Nitta, K. Kato, H. Tanida, K. Takeshita, S. Takahashi, M. Sano, H. Aoyagi, A. Watanabe, N. Nariyama, H. Ohashi, H. Yumoto, T. Koyama, Y. Senba, T. Takeuchi, Y. Furukawa, T. Ohata, T. Matsushita, Y. Ishizawa, T. Kudo, H. Kimura, H. Yamazaki, T. Tanaka, T. Bizen, T. Seike, S. Goto, H. Ohno, M. Takata, H. Kitamura, T. Ishikawa, T. Yokoyama, Y. Iwasawa, *J. Phys. Conf. Ser.* **2013**, *430*, 012020.
[12] Y. Wakisaka, Y. Iwasaki, H. Uehara, S. Mukai, D. Kido, S. Takakusgi, Y. Uemura, T. Wada, Q. Yuan, O. Sekizawa, T. Uruga, Y. Iwasawa, K. Asakura, *Journal of Surface Science Society of Japan* **2017**, *38*, 378–383.
[13] R. H. Terrill, T. A. Postlethwaite, C.-h. Chen, C.-D. Poon, A. Terzis, A. Chen, J. E. Hutchison, M. R. Clark, G. Wignall, *Journal of the American Chemical Society* **1995**, *117*, 12537–12548.
[14] aJ. Stöhr, *X-ray Absorption: Principles, Applications, Techniques of EXAFS, SEXAFS and XANES* **1988**, 443; bJ. Stohr, *NEXAFS Spectroscopy*, Springer **1992**; cF. Comin, J. E. Rowe, P. H. Citrin, *Phys. Rev. Lett.* **1983**, *51*, 2402.
[15] Y. Takagi, H. Wang, Y. Uemura, E. Ikenaga, O. Sekizawa, T. Uruga, H. Ohashi, Y. Senba, H. Yumoto, H. Yamazaki, S. Goto, M. Tada, Y. Iwasawa, T. Yokoyama, *Applied Physics Letters* **2014**, *105*, -.
[16] aM. G. Samant, G. Borges, O. R. Melroy, *Journal of The Electrochemical Society* **1993**, *140*, 421-425; bH. Nagatani, H. Tanida, M. Harada, M. Asada, T. Sagara, *The Journal of Physical Chemistry C* **2010**, *114*, 18583–18587; cT. Masuda, H. Fukumitsu, S. Takakusagi, W.-J. Chun, T. Kondo, K. Asakura, K. Uosaki, *Advanced Materials* **2012**, *24*, 268–272; dK. Murata, C. Kirkham, S. Tsubomatsu, T. Kanazawa, K. Nitta, Y. Terada, T. Uruga, K.-i. Nittoh, D. R. Bowler, K. Miki, *Nanoscale* **2018**, *10*, 295–301.
[17] aS. R. Brankovic, J. X. Wang, R. R. Adzic, *J.Serb.Chem.Soc.* **2001**, *66*, 887–898; bN. Kristian, X. Wang, *Electrochemistry communications* **2008**, *10*, 12–15; cW. Shuangyin, K. Noel, J. Sanping, W. Xin, *Nanotechnology* **2009**, *20*, 025605; dC. Xiu, W. Shengnan, J. Scott, C. Zhibing, W. Zhenghua, W. Lun, Li, *Nanotechnology* **2013**, *24*, 295402.
[18] S.-i. Nagamatsu, T. Arai, M. Yamamoto, T. Ohkura, H. Oyanagi, T. Ishizaka, H. Kawanami, T. Uruga, M. Tada, Y. Iwasawa, *J. Phys. Chem. C.* **2013**, *117*, 13094–13107.

[19] T. Kaito, H. Mitsumoto, S. Sugawara, K. Shinohara, H. Uehara, H. Ariga, S. Takakusagi, K. Asakura, in *PRiME(Pacific Rim Meeting) Vol. MA2012–02*, Honolulu Hawaii, USA, **2012**, p. 1651.
[20] F. Feiten, Y. Wakisaka, N. Todoroki, T. Wadayama, I. Sakata, O. Sekizawa, T. Uruga, Y. Iwasawa, K. Asakura, *J. Phys. Chem. C.* **in preparation**.
[21] M. Koichi, K. Christopher, S. Masaru, N. Kiyofumi, U. Tomoya, T. Yasuko, N. Koh-ichi, R. B. David, M. Kazushi, *Journal of Physics: Condensed Matter* **2017**, *29*, 155001.